Cloud Monitoring at the Pierre Auger Observatory

JOHANA CHIRINOS[1], FOR THE PIERRE AUGER COLLABORATION[2].

[1] *Michigan Tech. University, Houghton-MI, USA*
[2] *Full author list: http://www.auger.org/archive/authors 2013 05.html*

auger_spokespersons@fnal.gov

Abstract: Several methods are used to detect night-time cloud cover over the 3000 km^2 Pierre Auger Observatory, including lidars and laser sources. Here, we describe two methods. Infrared cloud cameras, installed at each of the four fluorescence detector sites, detect the presence of cloud within the fields of view of each fluorescence telescope every 5 minutes. Operating since 2002, an upgrade to improved hardware is underway. Secondly, a method has been implemented to use GOES-12 and GOES-13 satellites to identify night-time clouds over the Observatory. It has been validated using the Observatory's Central Laser Facility, which determines cloud cover above this facility. We develop cloud probability maps for the 3000 km^2 of the Observatory twice per hour and with spatial resolution of 2.4 km by 5.5 km and a database with the cloud probabilities for further analysis.

Keywords: Pierre Auger Observatory, ultra-high energy cosmic rays, atmospheric monitoring, clouds, satellites.

1 Introduction

The Pierre Auger Observatory employs several systems capable of detecting night-time cloud over the 3000 km^2 viewed by the observatory's fluorescence detectors, including two laser facilities within the array and lidar systems at the fluorescence detector (FD) sites [1, 2, 3]. Clearly, cloud is capable of attenuating fluorescence light from parts of air showers, resulting in dips in the measured longitudinal development profiles. In contrast, if a shower passes through a cloud layer, its intense Cherenkov beam may be scattered by the cloud resulting in an *increase* in light received at a fluorescence detector. Thus cloud detection is vital for reliable measurements of longitudinal shower profiles, the depth of shower maximum and primary particle energies, but also in searches for any effects of exotic particle physics on air shower development.

In this paper we discuss two key cloud detection methods which are used by the Observatory. The strength of our cloud detection lies in our ability to combine measurements from instruments with different capabilities.

2 Infra-red Cloud Cameras

The Pierre Auger Observatory utilizes infra-red cameras, located on the roof of each of the four main FD buildings, to observe the night-time sky conditions over the array. Being co-located with the fluorescence detectors, it is possible to directly associate cloud camera pixel directions with FD pixel directions, thus flagging detected showers that may be affected by cloud. Conservatively, showers may be disregarded if cloud is detected within any FD pixel viewing an event, or alternatively cloud camera data (giving cloud *direction*) may be combined with lidar or Central Laser Facility data on cloud *height* to locate the cloud in three dimensional space.

Each camera was installed shortly after the corresponding FD building was completed, between 2004 and 2007. Beginning in early 2013, each of the four infra-red cameras are being replaced by new radiometric cameras, which will be discussed in Section 2.4. What follows is a discussion on the current analysis for the original cameras.

2.1 Original Infra-red Cameras

Initially installed at the Pierre Auger Observatory were four Raytheon ControlIR 2000B infra-red cameras. The cameras were designed to measure infra-red light in the $7-14$ μm wavelength band, suitable for distinguishing warm clouds from the cold clear sky. Images captured by the cameras consist of 320×240 pixels spanning a $48^\circ \times 36^\circ$ field of view. Every five minutes during FD operation the cameras capture so-called *field-of-view* image sequences, which consist of five images covering the fields of view of the six FD telescopes. Each of the field-of-view sequences are used to evaluate the cloud conditions within the field of view of each FD pixel at the time of image capture. Additionally, a *full-sky* sequence of images is acquired every fifteen minutes which views the entire hemisphere above the FD site; the purpose being to aid shift-operators in determining real-time weather conditions near each FD site.

2.2 Image Artefacts

Over time, the quality of each camera deteriorates due to constant exposure to weather as well as simple wear and tear. Some image artefacts develop during operation which can be removed by periodic flat-fielding of the cameras. More difficult to handle are certain artefacts that have developed for some of the cameras.

Visible to some degree in most cameras is a consistent curved streaking artefact, possibly caused by a displacement of the internal *chopper* wheel during the panning of the camera (Fig. 1, left). Despite the artefacts retaining an unvarying shape from image to image, their baseline intensity appears to vary sporadically over long time scales as well being dependent on the local temperature at the camera, making it hard to apply a numerical correction for the artefacts. The development of these streaking artefacts has made previous algorithms, which utilise local weather conditions to estimate an expected camera signal for a clear

Figure 1: *Left*: Raw image from a *field-of-view* sequence taken from Coihueco on 2009/07/19 at 08:25 UTC. *Right*: The same image after having a clear sky template image removed from it. A signal threshold is then applied to create a binary cloud mask which is then mapped to the FD telescope pixels.

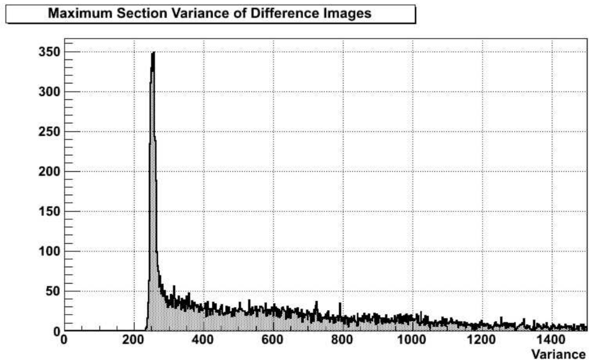

Figure 2: Distribution of the maximum section variance from the difference of consecutive images in time. A noticeable peak can be seen which is associated with clear sky images. Applying a cut corresponding to the tail of the peak can be used to distinguish clear and cloudy images.

sky, largely ineffective. For this reason we have developed a new method which can account for the most serious of artefacts yet still provide reliable cloud information.

2.3 Cloud Mask Generation

We have developed a new technique which can discriminate between pixels observing clear or cloudy sky within poor-quality images. The technique relies upon building a library of clear sky images which can be used as templates to be removed from each cloud covered image. The difference between the clear and cloudy images should result in enhancement of the cloud affected pixels.

To first determine which images are clear of cloud, each field-of-view sequence is compared to the next sequence of images in time. Any significant difference between the two sets of images may indicate that cloud is present. A small difference indicates the images may be clear. By splitting the difference images into $n \times m$ sections, small changes can be detected to provide higher precision in discriminating between clear sky and cloud.

Figure 2 shows the distribution of the maximum variance from all sections in many difference images. A clear peak can be seen associating with images with a low maximum section variance, indicating images that are most likely clear (no object movement). The tail of this peak can be used to differentiate between clear and cloudy images when combined with a mean signal cut to account for overcast images. A library of clear images is collected for a given (roughly two weeks) FD observation period.

For every other image, a weighting algorithm is applied to find the best match clear-sky template based on similar temperatures and time-of-day. The difference of the two images should result in a flat baseline image with areas of increased signals associated with cloud (Figure 1, right). Applying a simple threshold on the resultant image reveals the designated cloud and clear pixels. By averaging the information from each cloud camera pixel which shares the same direction as an FD pixel, we generate a *cloud index* for each FD pixel which represents the fraction of cloud in its field of view of that time. The result is a cloud camera database for use in shower analysis that contains cloud indices for every FD pixel at five-minute intervals.

2.4 New Infra-red Cameras

We are replacing the existing cloud cameras with Gobi-384 uncooled radiometric microbolometer array infra-red cameras. These cameras operate in the $8-14\ \mu$m wavelength band with a field of view of $50^\circ \times 37.5^\circ$ and produce images consisting of 384×288 pixels (Figure 3). The design of these new cameras prevents the occurrence of the main artefacts associated with the existing cameras, while also enabling absolute infra-red brightness temperature measurements of the sky. The cameras will be controlled using new LabView based software, to perform the same image capture sequences as described in Section 2.1. Using LabView for the hardware control system will allow a greater level of automation to be implemented into the image capture and camera calibration processes.

2.5 Future Work

The radiometric nature of the new cameras will allow for new cloud detection techniques. Of particular interest is the comparison of observed infra-red brightness temperatures with simulations, using GDAS (Global Data Assimilation System) [4] atmospheric profile data and atmospheric radiation transfer software. This will introduce an atmospheric profile dependent cloud detection threshold, which will help resolve the issue of high levels of water vapour being falsely detected as cloud, given that the camera wavelength range includes a water vapour emission band.

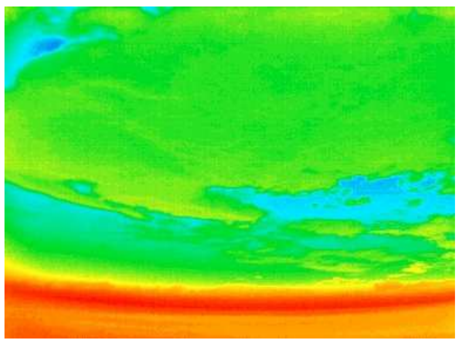

Figure 3: Example of a sky image taken with the radiometric Gobi-384 IR camera at the Los Leones FD site. Temperatures range from cooler (blue) to warmer (red).

3 Satellite Based Cloud Identification Method

3.1 Satellite

Besides the ground equipment at the Pierre Auger Observatory, we have developed a new method to identify nighttime clouds [5] from satellite images provided by the Geostationary Operational Environmental Satellites - GOES [6] (GOES-12, which was replaced by GOES-13 in April 2010). The satellite is stationed at 75 degrees West longitude. Its Imager instrument captures images of the South American continent every 30 minutes. Satellite images are produced in one visible band, and four infrared bands centered at wavelengths 3.9, 6.5, 10.7, and 13.3 μm and labeled Band 2, Band 3, Band 4 and Band 6, respectively.

When the pixels from the infrared band are projected on the ground at the Pierre Auger Observatory, the distance between the center of each pixel is about 2.4 km longitudinally and 5.5 km latitudinally. The visible band resolution is higher.

The raw data are publicly available from the NOAA website [7]. We selected a rectangular region centered at the Pierre Auger Observatory (S 35.6°, W 69.6°). These files contain information for 538 pixels. The data for each pixel in each Band i contain the latitude and longitude of the pixel center and, after calibration and some calculations, we obtain the pixel brightness temperature Ti. The brightness temperatures are the basic quantities for cloud determinations.

3.2 Ground-truthing with CLF

The most suitable ground instrument of the Auger Observatory for comparison with the satellite method is the Central Laser Facility (CLF). The cloudiness of the pixel encompassing the CLF can be monitored by the CLF. Every 15 minutes, the CLF produces a series of 50 vertical laser shots which are observed by all four FD stations. From the observed profile, clouds or clear sky over the CLF can be identified.

Typically, each satellite image is bracketed in time by two CLF shots, one 9 minutes before and other 6 minutes after the timestamp of the satellite image. The CLF pixel is tagged as “clear pixel” (“cloudy pixel”) if the two bracketing CLF profiles were both identified as “clear CLF” (“cloudy CLF”) states. This is to eliminate short-term cloud cover changes.

We used one year of data. For these studies, we arbitrarily chose data from 2007.

3.3 Cloud Identification Method

For our method, we selected the difference between the unattenuated brightness temperatures (T2-T4) and the highly attenuated brightness temperature (T3). These satellite-based variables show a separation between “clear pixel” and “cloudy pixel” and only a mildly dependence on ground temperature, minimizing the dependence on daily, weekly or seasonal temperature variations of the method.

In Figure 4, we plot T3 vs. T2-T4 using data of the CLF pixel in 2007. The tagged “clear pixel” (open blue circles) congregate in the upper left quadrant. The tagged “cloudy pixel” (red stars) form an anti-correlated linear feature occupying the center.

This study can be extended for any of the other 538 pixels of the satellite image provided that we can get T2, T3 and T4 for that pixel and we consider that the geographical and meteorological conditions of the other 538 pixels are similar to the conditions of the CLF pixel.

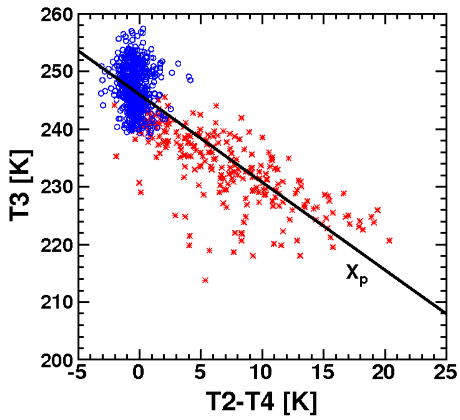

Figure 4: T3 vs. T2-T4 of the CLF pixel in 2007. Open blue circles (red stars) were tagged “clear pixels” (“cloudy pixels”) from the CLF study. X_p is the principal axis of the fitted line.

We project the data from Figure 4 onto the principal axis X_p described by the fitted line to the overall distribution. In Figure 5, we show one-dimensional histograms of the clear (black thick line) and cloudy (red dashed line on the right) tagged data with respect to the position along the principal axis X_p. Also shown is a clear pixel “normalized” histogram (blue thin line on the left) scaled to have the same area as the cloudy pixel histogram. Suitably normalized, these histograms represent probability distribution functions, yielding the probability of identifying a cloudy (clear) pixel for a given value of the principal axis coordinate. Using information from both the reduced clear histogram and the cloudy histogram, we assign a cloud probability for each bin along the principal axis X_p by dividing the number of cloudy entries by the sum of the cloudy and clear entries.

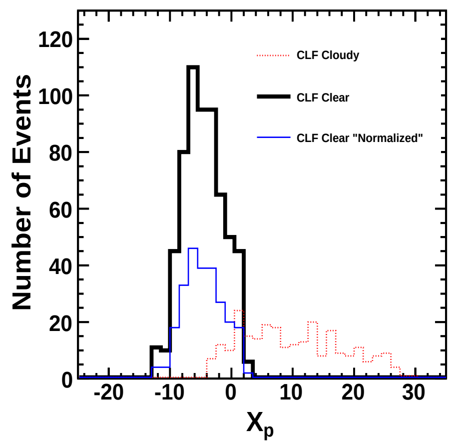

Figure 5: Clear (black thick line), clear “normalized” (blue thin line on the left), and cloudy (red dashed line on the right) tagged distributions on principal axis X_p.

3.4 Applications for the Auger Observatory

We have generated cloud probability maps (see Figure 6) for each satellite image available from all the FD running nights since 2004. In addition, using these maps, nightly animated maps were created. These maps (especially the animated versions) are useful in visualizing the cloud cover during particular cosmic ray events. This helps us to distinguish shower profiles distorted by clouds from unusual shaped shower profiles that could correspond to exotic or rare events.

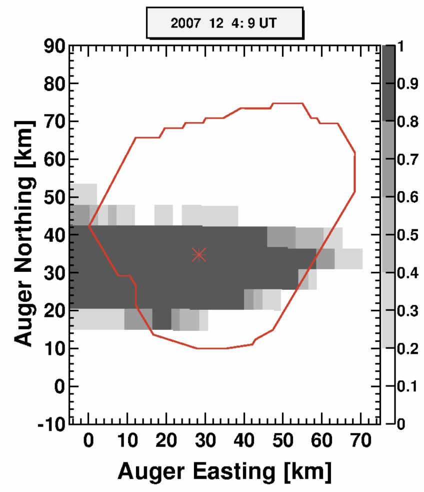

Figure 6: Example of a cloud probability map of the Pierre Auger Observatory. Pixels are colored in accordance with the gray scale to the right of the maps. Shown are the borders of the SD (red) and the CLF (red star).

The cloud probabilities for every pixel of the satellite images since 2004 are provided in one of the Auger atmospheric databases for further reconstruction analysis of the cosmic ray data. In the database, the cloud probability is digitized with cloud probability indexes ranging from 0 to 4. For all the cases when the cloud probability of the corresponding bin is between 0 and 20 %, we consider the pixel as clear and we assign 0 to the cloud probability index (CP = 0). For all the cases when the cloud probability of the corresponding bin is between 80 and 100 %, we consider the pixel as cloudy and we assign 4 to the cloud probability index (CP = 4). We assign cloud probability indexes between 1 and 3 for the intermediate cases.

Using this database, the plan is to increase the efficiency of the data analysis cuts for the cloudy nights for the cosmic ray analysis. Also, candidates of exotic events will be vetoed, when these events developed within cloudy pixels.

3.5 Reliability of the method

As we can see in Figure 5, there is a small overlap in the distributions. One contribution to the overlap may come from the fact that the CLF data and the satellite image are not precisely simultaneous. Another contribution comes from the fact that the CLF laser beam illuminates an area less than 100 m across as compared to the size of square kilometers of the satellite pixel. The rare clouds higher than the maximum field of view of the FD (14 km) contribute to this overlap since they can be identified by the satellite but not by the CLF. The spatial uncertainty in the satellite pixel location could contribute also to the overlap since the raw data at NOAA do not include the spatial correction in the coordinates of the satellite pixel.

Another reason for the overlap could be that the satellite may be less sensitive than the CLF to certain types of clouds such as the optically thin clouds. Optically thin clouds are not important for distortions due to absorption, but could indeed act as side-scatterers. The CLF is a perfect device to simulate such side scattering. It is possible by averaging over 50 CLF tracks to detect clouds that would cause a less than significant effect on a single cosmic ray event but would still cause a statistically significant change to the averaged CLF profile. However, the goal of this study is only to identify night-time clouds and not to discriminate between cloud type or altitude.

For the atmospheric database, we defined CP = 0 for clear pixels and CP = 4 for cloudy pixels. With these cuts, we are conservative for not incorporating false positives. CP = 0, means cloud probabilities for each corresponding bin of less than 20 %. Using all the bins below this cut, we get a total cloud probability of 4 %. CP = 4 means cloud probabilities for each corresponding bin of more than 80 %. Using all the bins above this cut, we get a total cloud probability of 99 %. However, our method could be applied with different cuts, depending on the needed goal.

4 Conclusions

We have described two of the four cloud detection methods employed at the Pierre Auger Observatory. Infra-red cloud cameras situated at each of the four fluorescence sites can directly map cloud directions onto the FD pixel directions which can then be used to veto cloud-affected air showers. The new GOES-satellite based method provides straightforward cloud detection over the entire array that can also be used to veto events. The Observatory relies on the combination of *all* of its cloud detection instruments, including the central laser facilities and lidars at the FD sites, for cloud information. This is especially the case for studies very sensitive to cloud effects, such as the search for exotic physics in the development of air shower cascades.

Acknowledgment: This work was in part supported by the Department of Energy (Contract No. DE-FG02-99ER41107) and other agencies involved in funding of the construction and operation of the Pierre Auger Observatory.

References

[1] The Pierre Auger Collaboration, J. Abraham et al., *Astroparticle Physics* **33** (2010) 108.
[2] The Pierre Auger Collaboration, J. Abraham et al., *JINST* **8** (2013) 4009.
[3] L. Valore for the Pierre Auger Collaboration, *Measuring Atmospheric Aerosol Attenuation at the Pierre Auger Observatory*, this conference.
[4] The Pierre Auger Collaboration, J. Abreu et al., *Astroparticle Physics* **35** (2012) 591.
[5] J. Chirinos for the Pierre Auger Collaboration, *Eur. Phys. J. Plus* **127** (2012) 93.
[6] GOES Project Science, http://goes.gsfc.nasa.gov .
[7] NOAA CLASS, http://www.class.ncdc.noaa.gov/saa/products/welcome .